Texture evolution in large strain simple shear deformation of high density polyethylene

Z. Bartczak*, A. S. Argon† and R. E. Cohen
Massachusetts Institute of Technology, Cambridge, MA 02139, USA
(Received 1 February 1993; revised 11 January 1994)

The deformational behaviour of linear high density polyethylene (HDPE) in simple shear to large strains and the mechanisms involved in this deformation were investigated. The specimens were sheared at a constant rate at room temperature. The structure and morphology of the samples of HDPE deformed to various permanent shear strains up to 6.3 were studied using wide-angle and small-angle X-ray scattering and transmission electron microscopy. The results show that the simple shear deformation of HDPE is controlled by crystallographic slip mechanisms, mostly the (100)[001] chain slip supported by the (100)[010] transverse slip and (010)[001] chain slip. The crystallographic deformation mechanisms were found to be active in the whole range of the strain history. At strains up to 3.0 the deformation by these mechanisms is supported by shear in the amorphous interlamellar layers (interlamellar sliding) which also alters the orientation of the crystalline phase. This sliding appears to be partially reversible on unloading. At moderate strains chain slip becomes unstable, which causes the localization of deformation within numerous fine shear bands. Further deformation concentrated in bands leads to the destruction of the crystalline lamellae and the transformation of the sample morphology into a microfibrillar one at a shear strain near 4.3. Further deformation, mostly by chain slip, in the crystals arranged after their fragmentation into microfibrils results in a sharp, nearly axial texture with the chain axis c tilted a few degrees away from the direction of shear.

(Keywords: texture evolution; shear deformation; HDPE)

INTRODUCTION

Plastic deformation of semicrystalline polymers has been studied from many aspects in the past. It is now well established that the principal mechanisms involved in the process are of crystallographic nature[1–3]. However, this plastic deformation appears to be a very complex process, involving additionally several other deformation mechanisms specific for particular morphologies of semicrystalline polymers. This is especially the case for deformation of unoriented virgin samples exhibiting a complicated multilevel morphology. Because of such complexity the deformation path of semicrystalline polymers is presently not completely understood, and many questions still remain in spite of a large amount of experimental and theoretical work performed over the past two and a half decades.

In order to model successfully the very complex process of plastic deformation in semicrystalline polymers, it is necessary to collect still more quantitative information from experimental studies. The deformation of semicrystalline polymers, particularly high density polyethylene (HDPE), in the tensile mode has been studied extensively in the past[1–3]. Deformation by compression has been studied to a much smaller extent. To rectify this deficiency we have recently investigated in detail the plastic deformation of HDPE under plane strain compression[4] and uniaxial compression[5]. In our recent studies on HDPE under compression[4,5], we have demonstrated that the widely accepted model of plastic deformation devised by Peterlin[6], known as 'micronecking'[6], is not essential for large strain deformation. It occurs only in tensile deformation which promotes microstructural cavitation and acts primarily as an impediment to fundamental understanding. It is absent in compressive flow.

In contrast, relatively little attention has been given in the past to deformation by shear[7,8], which is in fact the basic deformation mode at the microscopic level. The aim of the present work was to study in detail the plastic deformation process, including the resulting changes in crystallite orientation and morphology of bulk HDPE, in initially spherulitic form, subjected to large strain deformation by simple shear. Because the deformation of polymers in the shear mode is macroscopically homogeneous, without any discontinuities like necking observed in tensile experiments, it is possible to study, step by step, the development of deformation textures and morphology changes resulting from plastic deformation over the whole range of strain history, and therefore gather additional important information on the plastic deformation process and the mechanisms

* Present address: Centre of Molecular and Macromolecular Studies, Polish Academy of Sciences, Sienkiewicza 112, 90-363 Lódź, Poland
† To whom correspondence should be addressed

0032-3861/94/16/3427-15

involved. Linear high density polyethylene was chosen as the material for this study because of the large amount of existing experimental information and relatively high degree of knowledge of the plastic deformation mechanisms active in this polymer.

EXPERIMENTAL

Materials and sample preparation

The material used in this study was high density polyethylene (HDPE), PETROTHENE™ LS 606-00, supplied by Quantum (USI Division, Cincinnati, OH, USA). Its molecular weight M_w was 55 000 g mol^{-1} with a polydispersity M_w/M_n of 4.8; the melt flow index was 9–11 g per 10 min (ASTM D-1238) and the density was 0.941–0.980 g cm^{-3}.

The polymer pellets were compression moulded at 180°C and 100 atm pressure to form a plate of 20 mm thickness. From the moulded plates the outer layers (at least 5 mm from each side) were removed by machining. As revealed by X-ray measurements, the processed material had an overall crystallinity exceeding 70% and no traces of any crystallographic orientation anisotropy, which might be a result of the compression moulding. In the next step, the specimens for simple shear experiments were machined out from the core plates, as sketched in *Figure 1*. During machining of the specimens both the polymer and the cutting tool were cooled continuously with water in order to minimize possible changes of the morphology at specimen surfaces. Finally, the finished machined parts of the specimens were carefully polished with fine aluminium oxide powder (particle size 0.05 μm) suspended in water.

The shape of the specimens was designed to limit the shear deformation only to a narrow reduced part and to avoid any deformation of the material within the much thicker gripped portions. In the gripped parts of the specimen, bolt holes for attachment to the shearing device were drilled. The tightened bolts improved the gripping of specimens under load. The dimensions of the shear specimens are shown in *Figure 1*. The specimens were made in two sizes: large specimens were designed to be deformed in an Instron testing machine and then studied by X-ray techniques and transmission electron microscopy in the unloaded, fully relaxed state, whereas the small specimens were designed to be deformed in a small shearing machine placed inside the X-ray camera where they were to be deformed during the X-ray exposures. In the case of the large specimens, the relatively large width of the calibrated portion of the specimen was necessary in order to obtain sufficiently large deformed samples for X-ray studies of crystal orientation by the pole figure technique. The width of the second type of specimen could be significantly smaller because in this case probing was by a fine point focused X-ray beam in the transmission mode. The dimensions of the specimens of both types were selected according to the limits for simple shear specimens as discussed by G'Sell *et al.*[7] in order to make the shear deformation more homogeneous and minimize other unwanted deformation modes.

Large shear specimens were deformed using an Instron testing machine (model 4201) equipped with a special simple shear device of a design similar to the device described elsewhere by G'Sell *et al.*[7]. Prior to deformation the calibrated part of the specimen was printed with straight marker lines perpendicular to the expected direction of shear. The specimens, firmly gripped in the shear device, were subjected to a constant nominal local shear rate of 1×10^{-3} s^{-1} at room temperature. The experimental stress–strain curves were corrected for the compliances of the testing machine and the grips. Each specimen was deformed to a desired shear strain, left under load for 15 min and then unloaded. Finally, the specimen was allowed to relax and recover a part of the strain. In the deformed specimen a part (usually the centre) in which the marker lines remained completely straight, i.e. where the macroscopic deformation was truly simple shear, was selected for further structural studies. The local shear strain in that part was calculated from the tangent of the measured rotation angle of the appropriate marker line.

Small shear specimens were deformed directly in the X-ray camera using a small shearing machine made of a rigid frame and a mobile part guided by a linear slider, actuated by a lead screw. The gripped specimen was sheared to the desired shear strain by driving the lead screw of the testing machine. The shear strain rate was controlled in this experiment only through rough, manual control of the displacement rate of the grips. The experiment was designed to monitor the changes in crystallite orientations by X-ray techniques during the deformation process under load, during relaxation and in the unloaded and relaxed state.

X-ray measurements

The overall orientations of the crystallographic planes of the original and sheared samples, cut out from the Instron specimens after their deformation, were determined by means of an automated, computer-controlled Rigaku wide-angle X-ray scattering (WAXS) system consisting of a pole figure device associated

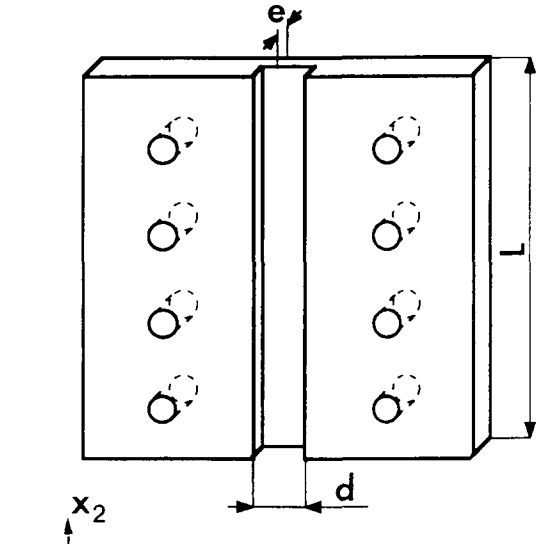

Sample:	Large	Small
L (mm)	100	40
d (mm)	9	2.5
e (mm)	3	1.5

Figure 1 The geometry of the specimen for planar simple shear

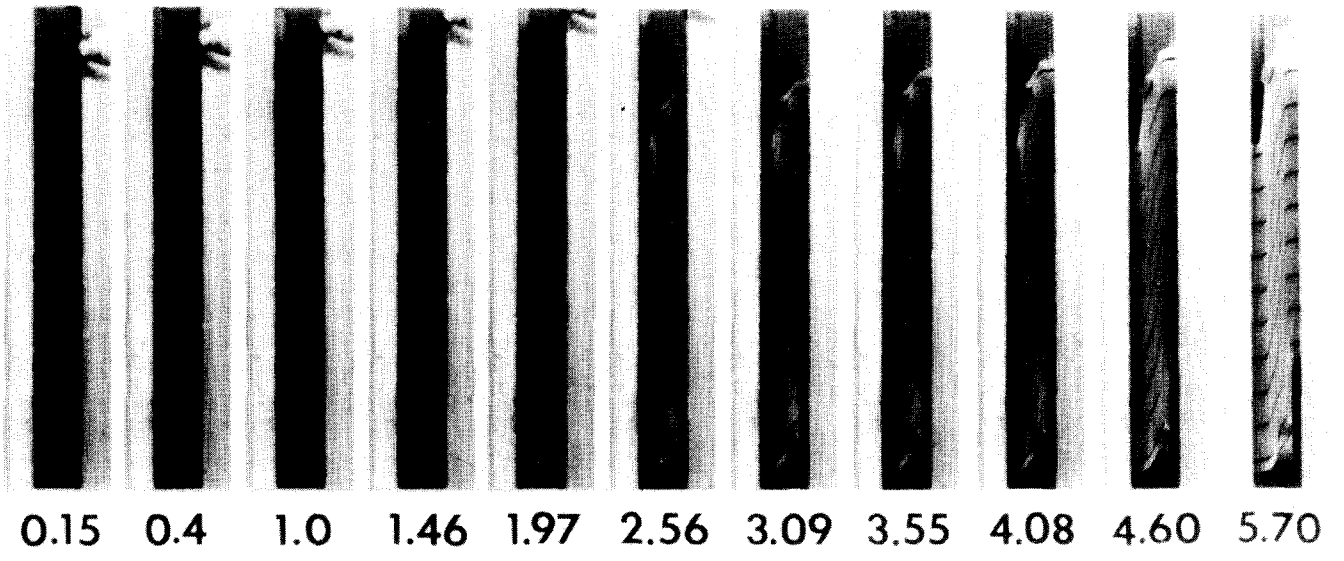

Figure 2 Photographs of a shear specimen taken during its deformation. The actual shear strain is shown below each photograph

with a wide-angle goniometer coupled to a rotating anode X-ray generator operating at 50 kV and 60 mA (CuKα radiation, filtered electronically and by an Ni filter). The complete pole figures were obtained for projections of Euler angles of sample orientation with respect to the incident beam, with the angle α varying from 0° to 90° in 5° intervals and β varying from 0° to 360° in 5° steps. The construction of complete pole figures required the connection of the X-ray data collected in both transmission and reflection modes, where the connection angle α_c was 40°, except for the (002) pole figure for which α_c was 30°. The slit system of the diffractometer was selected to measure the integral intensity of the appropriate diffraction peak. The diffraction data were collected and the necessary corrections for background scattering and sample absorption were calculated using the DMAXB software (Rigaku, USA). The pole figure plots were generated by the program POD, a part of the popLA package (Los Alamos National Laboratory, Los Alamos, NM, USA)*. The pole figures for the following crystal planes of orthorhombic polyethylene were constructed: (110), (200), (020) and (002).

The changes in lamellar orientation in the sheared samples were studied by means of small-angle X-ray scattering (SAXS). These SAXS measurements were performed using another system incorporating a Siemens two-dimensional position sensitive detector and a second Rigaku rotating anode, fine point X-ray generator emitting CuKα radiation and operating at 40 kV and 30 mA. The primary beam was collimated by a two-mirror collimating system consisting of Ni mirrors. The specimen to detector distance of the SAXS system was 2.3 m. The scattered X-ray path between specimen and detector was enclosed by a large aluminium tube with Kapton windows, filled with helium to minimize background scattering. The time for data collection was usually 10 min, although much shorter exposure times were also used.

Changes in lamellar orientation were also studied by SAXS on the small shear specimens deformed directly in the SAXS camera using the small shearing machine so that the specimen remained under load during the measurement; these specimens were also examined after load release. The exposure time was shortened to less than 30 s. Using the same experimental set-up, but with a short sample to detector distance (8 cm), the WAXS patterns were recorded for specimens under load and after load release. These specimens for WAXS were sheared to strains very close to those imposed on the specimens examined by SAXS.

Microscopy

The morphologies of the original and sheared specimens were examined by means of transmission electron microscopy (TEM). For the purpose of these studies, all the initial and deformed specimens were first stained and fixed in chlorosulfonic acid at 60°C for 20 h according to the procedure described by Kanig[9]. After staining, ultrathin sections were cut out from the samples. The sectioning of stained samples was performed at room temperature using an LKB Ultramicrotome V equipped with freshly prepared glass knives. The sections were examined using a Philips 300 transmission electron microscope operating at 100 kV.

RESULTS

Macroscopic behaviour

Figure 2 shows photographs of a large shear specimen printed with marker lines, taken during its deformation in an Instron testing machine. The photographs were taken at increasing overall shear strain, as marked on each photograph. This overall shear strain, in contrast to the local shear strain, was defined as the ratio of the crosshead displacement to the width of the reduced part of the specimen. The evolution of the shape of initially straight marker lines shows that the deformation of the specimen is practically limited to the narrow part of the specimen, but that the deformation, especially at higher overall shear strains, does not develop homogeneously over the whole specimen length. In the central part of the specimen the marker lines remain straight up to a high overall strain, tilting gradually towards the direction of shear with increasing overall

* We are grateful to Professor L. Anand of the MIT Mechanical Engineering Department for providing us with this plotting program

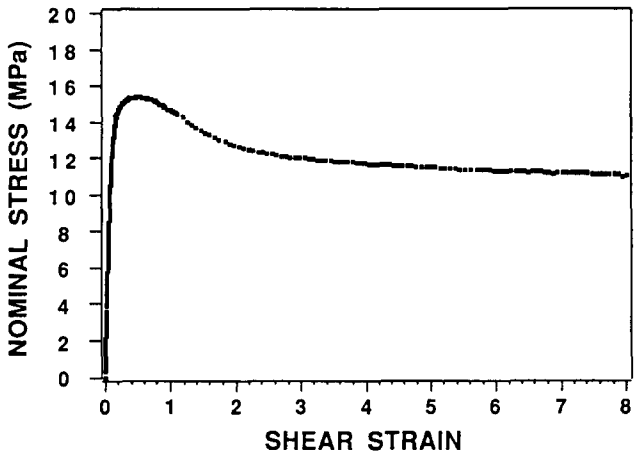

Figure 3 The dependence of the nominal shear stress on the overall shear strain for the large Instron specimen

strain. This, together with the results of supplementary measurements of the specimen thickness and width, suggests that the mode of deformation in this part of the specimen was exclusively the intended planar simple shear. However, the character of the deformation at both ends of the narrow section of the specimen was more complicated and the shear there was accompanied by other deformation modes; the marker lines became curved with increasing strain and the material close to the specimen ends was evidently deformed additionally in tension and compression. Some bending near specimen ends could also be observed at the highest strains. The inhomogeneities of the strain start to develop at an overall shear strain of less than 1.0, and increase significantly with increasing overall strain. The unwanted tensile and compressive strains near specimen ends are the result of the presence of normal stresses caused by grip constraints[7]. To minimize their influence on the overall deformational behaviour, the ratio of the specimen length to the width should be as large as possible, at least 15 according to the analysis of G'Sell *et al.*[7]. In the case of our Instron specimens this ratio was smaller (in the region of 7) because of the need to compromise between the large specimen width required for X-ray studies and the length limited by the capacity of the testing machine. Thus, the zones in which the shear deformation was disturbed by the presence of normal stresses were a relatively larger fraction of the length of the narrow shear zone than that observed previously by other investigators[7,8]. We note, however, that in the case of the small specimens, having a large length to width ratio for the narrow shear zone, the end effects discussed above affected a substantially smaller fraction of the shear zone.

The other feature of the deformation of the large specimens was whitening in the deformed polymer from an overall shear strain starting at 1.0. This whitening was strongest at the specimen ends and spread out over the whole gauge zone with increasing overall strain. Such behaviour was most probably the result of the previously discussed unwanted tensile deformation of the specimen, initiated near the ends of the shear zone, which causes cavitation of the deformed polymer. This cavitation was confirmed by the SAXS measurements reported below. Again, we note that in the small specimens, in which the tensile deformation was limited to a smaller area and was much less intense, such a strong whitening of the material was not observed, and in the middle part these specimens remained practically free of cavities up to high overall strains.

The shear stress *versus* overall shear strain curve corresponding to the deformation of large specimens in the Instron machine at room temperature is presented in *Figure 3*. It is seen that after the initial linear elastic stage, plastic deformation starts to develop at an overall shear strain above 0.1. At an overall strain near 0.3 the curve reaches a maximum, followed by a noticeable stress decrease with increasing strain up to 2.5. Above that strain the shear stress continues to decrease, albeit at a much slower rate. No strain hardening was observed. Such behaviour is different from that reported previously by G'Sell *et al.*[7,8], who observed a similarly shaped stress–strain curve up to a shear strain near 2.5, but reported a region of slight strain hardening for higher strains. The lack of strain hardening in simple shear is commonly observed and is also predicted by texture simulations[10]; nevertheless, it could also be influenced by cavitation of the polymer at high strains. Formation of cavities along the direction of the maximum stretch will soften the sheared material. This effect, however, is not considered to be dominant here.

The specimens deformed by shear to various strains showed substantial amounts of strain recovery after load release. The instantaneous elastic recovery was followed by a second prolonged and time dependent recovery process, which was quite intense within the first hour after unloading, then slowed down, and was almost complete within several hours, but needed as much as a few days to cease completely. This process is illustrated in *Figure 4*, where the transient plastic strain, as measured just after elastic recovery (shown by open squares), and the nearly permanent plastic strain, as measured 24 h after unloading (shown by filled squares), are plotted as a function of the strain imposed on the sample under load. It is seen that the elastic part of the strain recovery is constant, independent of imposed strain, whereas the

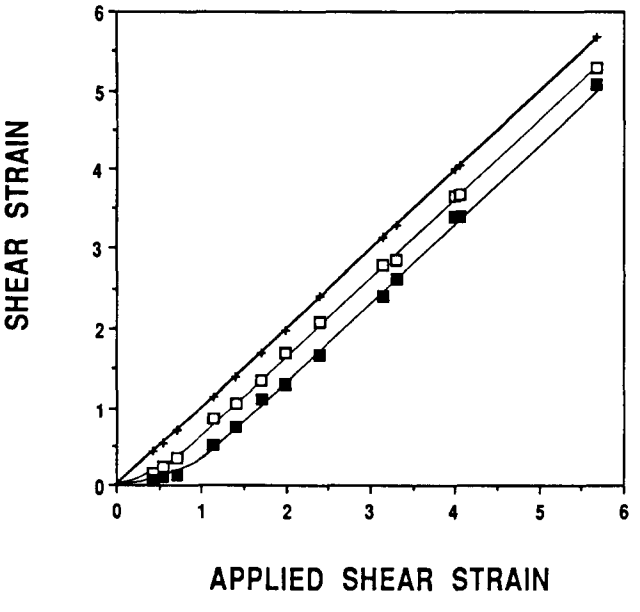

Figure 4 The dependence of the actual strain on the applied strain: (——) shear strain measured under load; (□) shear strain measured immediately after sample unloading; (■) shear strain measured 24 h after unloading

Table 1 Deformation parameters of the samples studied

Specimen number	Overall shear strain under load	Permanent local shear strain in selected area
1	0.42	0.08
2	0.71	0.16
3	1.40	0.42
4	1.70	1.00
5	2.40	1.40
6	2.98	1.80
7	4.05	3.00
8	5.67	4.30
9	7.46	6.30

time dependent component is a function of the applied strain; it increases initially from 0 to about 0.3 with increasing applied shear strain up to 0.7 (where the corresponding permanent shear strain is around 0.1), and then the amount of recoverable strain remains nearly constant. Clearly, this time dependent strain recovery is associated not only with the release of residual stresses caused by plastic inhomogeneities but also with the undoing of some inelastic deformation. We have previously observed similar recovery behaviour in samples of uniaxially compressed HDPE[5], where the recovery was the result of reverse interlamellar sliding after unloading of the sample.

X-ray results

From the large Instron specimens after their deformation to desired shear strains and after 10 days of strain recovery, smaller samples were selected for structural studies from the central portions of the Instron specimens, where the simple shear was found to be a homogeneous, undisturbed deformation mode. Two adjoining pieces 6–7 mm in width and 10–15 mm in length were cut out and then glued together side by side in order to obtain a sufficiently large sample for pole figure measurements. *Table 1* shows the shear strains of samples used for such further investigations.

The wide-angle diffraction curves obtained for deformed samples (not shown here) demonstrate that most of the crystals present in the samples are orthorhombic. The fraction of monoclinic crystals in every deformed sample was practically as low as in the undeformed material and did not vary with increasing shear strain. This suggests that martensitic transformations can be excluded as an important deformation mechanism active in the shear of HDPE.

Figures 5a–i show the pole figures constructed for the deformed samples from the reflections of the (110), (200), (020) and (002) crystallographic planes of the orthorhombic polyethylene crystals. For better visualization of the orientation in the early as well as late stages of deformation, the pole figures of particular samples were plotted with various intensity scales. In each pole figure the x_3 direction (for a definition of the coordinate system see *Figure 1*) is perpendicular to the projection plane and the direction of the imposed shear is marked by arrows. Additionally, the pole figures in *Figures 5a–i* present the WAXS diffraction patterns recorded in the transmission mode with the X-ray beam parallel to the x_3 axis. *Figure 5a* shows that from the early stages of plastic deformation (permanent shear strain $\gamma = 0.08$) the normals to the 200 planes, i.e. the a axes of the crystals, tend to concentrate in the x_1–x_2 plane, perpendicular to the x_3 axis and tilted about 45° to the shear direction x_2. At the same time the normals to the 020 planes, i.e. the b axes, outline a weak and broad orientation maximum, moving near to the equator of the pole figure and about 90° from the maximum of the [200] orientation. The normals to the 002 planes (molecular axis, c) start to rotate away from the x_3 direction. At higher shear strains, up to $\gamma = 1.0$ (see *Figures 5b–d*), the orientation maximum of the a axis rotates slowly towards the x_1 axis while remaining on the equator and becoming increasingly better defined with increasing strain, whereas the orientations of the b and c axes undergo some evolution and become only more gradually better defined. At $\gamma = 0.16$ (see *Figure 5b*), the previously weak orientation maximum of the normals to the 020 planes becomes stronger and starts to split into two parts. In each part the orientation tends towards the x_3 direction. This defines two planes of orientation for the b axes of the crystallites, crossing each other along x_3 (see *Figure 5d*). These planes give the impression of rotation around the x_3 axis towards the x_2–x_3 plane while the shear strain increases. However, the rates of rotation of these planes seem to be different. Similarly, but in a clearer way, an orientation pattern develops for the 110 planes (*Figures 5c* and *5d*). At the same time the clear bimodal orientation of the c axis, matching the orientations of the 020 and 110 planes, emerges in the equatorial zone of the (002) pole figure (*Figure 5d*).

A closer examination of the pole figures for the 200 planes, supported by examination of the WAXS patterns, indicates that each of the observed orientation maxima in fact consists of two orientation clusters, similar to the orientation of the other planes. The maxima corresponding to these clusters strongly overlap, which gives the impression of a single orientation cluster for the a axis. Such strong overlapping of the orientation maxima in the pole figures is an experimental artefact, at least in part, resulting from the location of the (200) diffraction peak on the shoulder of the (110) peak, which probably influences the measured intensities of the diffractions from the 200 planes.

At a permanent strain of $\gamma = 1.0$, one of the planes including the orientation maxima of the 020 and 110 plane normals stabilizes its position at about 85° with respect to the shear direction x_2 and does not rotate any further with increasing strain. This coincides with the stabilization of the position of one pair of [001] maxima (c axis) at 5° from the direction of shear. The evolution of the (200) pole figures suggests also that one pair of overlapping maxima for the a axis orientation does not change its orientation further, which is consistent with the behaviour of the other crystallographic axes.

At the strains $\gamma = 1.4$ and 1.8 (*Figures 5e* and *5f*), the maxima of the (200) orientations slowly spread out from the previous equatorial plane positions towards the x_3 direction, which suggests some rotation of the crystals around their c axes. The pole figures of the 110, 020 and 002 planes now clearly show a bimodal orientation distribution. The first and stronger mode constitutes the crystals oriented quite sharply with their c axes in the x_1–x_2 plane, about 5° away from the x_2 shear direction, while the a and b axes are distributed in the plane perpendicular to the strong c direction cluster. The maximum of the a axis orientation distribution in that

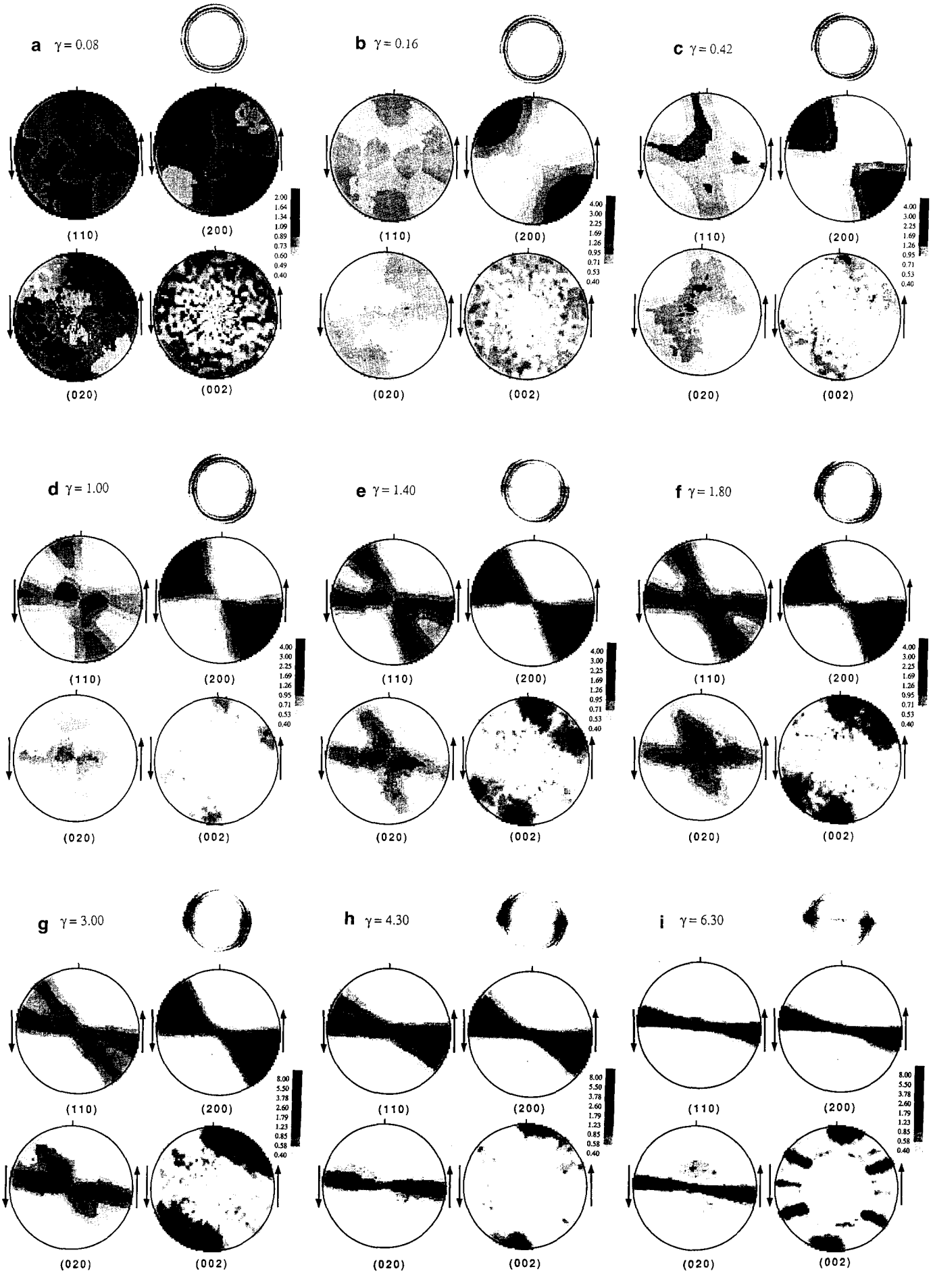

Figure 5 The WAXS diffraction patterns including the (110) and (200) reflections and the pole figures of the (110), (200), (020) and (002) planes determined for the samples deformed to permanent shear strains of (a) 0.08, (b) 0.16, (c) 0.42, (d) 1.0, (e) 1.4, (f) 1.8, (g) 3.0, (h) 4.3 and (i) 6.3

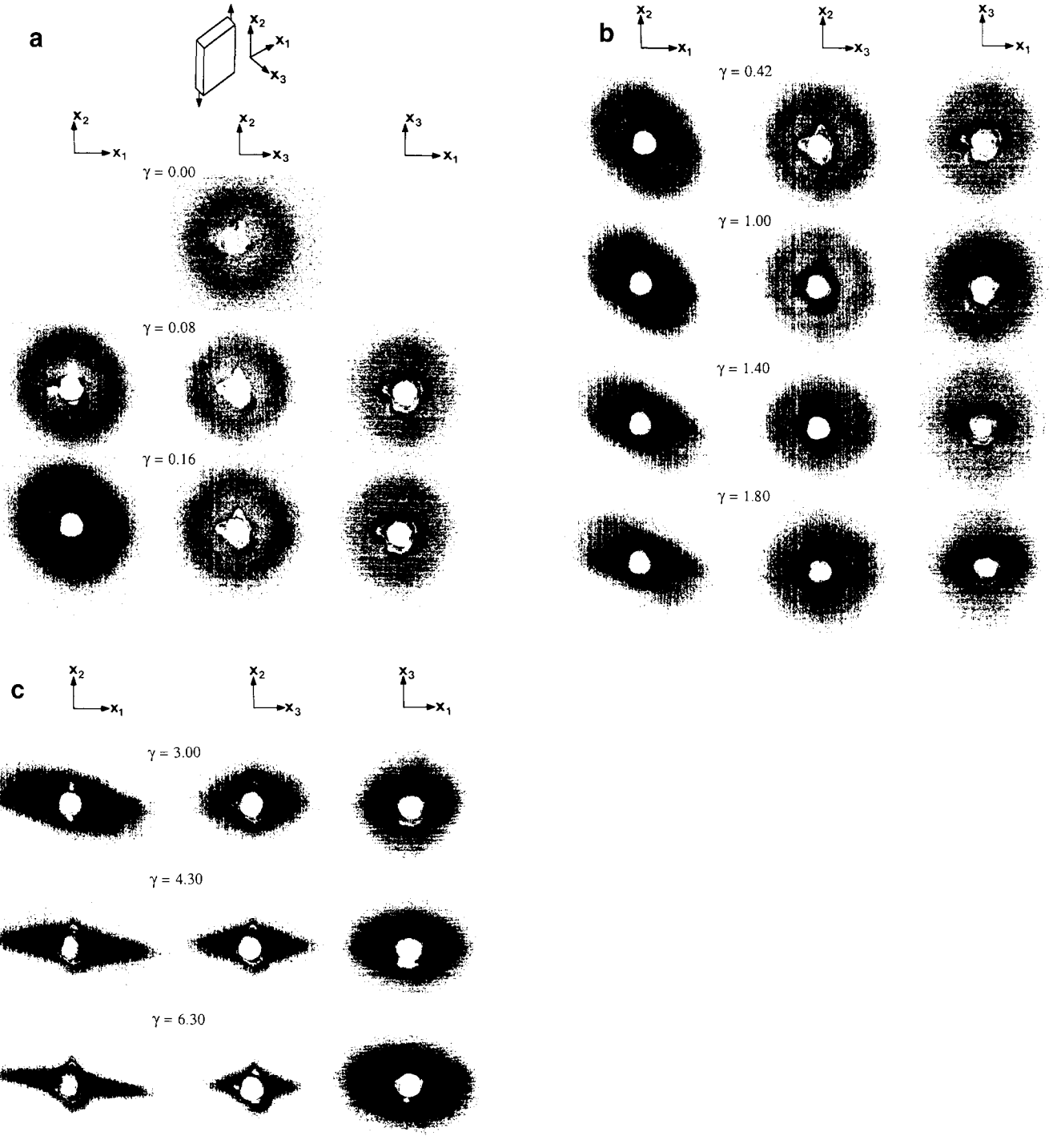

Figure 6 The SAXS patterns of the samples deformed to the given permanent shear strains as viewed from the x_3 (left-hand column), x_1 (central column) and x_2 (right-hand column) directions

plane is centred on the equator of the pole figure; the maximum of *b* spreads out in a plane around the x_3 direction. The second mode (cluster) of crystal orientations shows features similar to the first one, but the more diffuse maximum of the *c* axis distribution for $\gamma = 1.4$ is located about 40° from the shear direction and still rotates towards this direction as the shear strain increases. Simultaneously, with increasing shear strain the fraction of crystals oriented according to the first mode grows markedly, whereas the maxima for the second orientation mode slowly fade in the pole figures, and finally at $\gamma = 4.3$ this mode vanishes completely (see *Figures 5h* and *5i*).

At high shear strains ($\gamma = 3.0$, 4.3 and 6.3; *Figures 5g–i*), the previously mentioned elongation of the maxima of the distributions of the *a* and *b* axes in the plane perpendicular to *c* continues, even intensifies, and finally at $\gamma = 6.3$ the distributions of the (200), (020) and (110) poles in their common plane become almost uniform (see *Figure 5i*). In this way, the texture produced by shear at high strain is close to a sharp axial fibre texture with the *c* axis tilted away from the shear direction by 5° in the x_1–x_2 plane and (*hk*0) poles distributed in the plane perpendicular to *c*, similar to a drawn fibre texture.

Figure 6 presents the SAXS patterns for the specimens deformed to the specified permanent shear strains,

determined after unloading and strain recovery (the samples used for SAXS were the same as for pole figure measurements). For each specimen three SAXS patterns were taken, each with the incident beam parallel to one of the sample reference axes (see insets in *Figures 1* and *6*). The initial undeformed sample gives the uniform ring scattering independent of orientation with respect to the incident beam. With shear strains increasing up to $\gamma = 1.0$, the SAXS pattern recorded with the X-ray beam along the x_3 direction turns into an oval shape with its longer axis rotating away from the shear direction with increasing strain, while the patterns viewed from the x_1 and x_2 directions remain practically unchanged in shape and size. The long period as determined along the longer axis in the elliptical pattern viewed from the x_3 direction decreases a little compared to the long period of the undeformed specimen, whereas that determined along the shorter axis remains nearly constant for $\gamma = 0.08$ and 0.16 and increases slightly with further strain.

At $\gamma = 1.4$, the pattern viewed from the x_1 direction also becomes elliptical, with the shorter axis oriented along the shear direction x_2, which indicates a small increase in the long period of those lamellae with normals oriented near x_2. The long axis of the ellipse has the same length as the diameter of the ring observed at lower strains. The pattern observed along x_2 still forms a circle with relatively unchanged size and that along x_3 resembles now a narrow ellipse or, more likely, a tilted and diffuse two-point pattern. The long axis of this pattern continues to rotate away from the shear direction compared to smaller strains. The scattered intensity of the lamellar structure in all patterns is now lower than for smaller shear strains, and continues to decrease even more for higher strains. Moreover, for the strain discussed here, a new, very strong form of scattering appears in the equatorial zones of the SAXS patterns, especially in the pattern observed along the x_3 axis. The intensity of that scattering mode decreases strongly with increasing scattering angle. All the features of this mode of scattering are very similar to those of the scattering characteristic for oriented elongated voids incorporated in the sample. This mode of scattering becomes much stronger with further increases in strain. For $\gamma \geqslant 3.0$, the observed equatorial streaks become dominant in the scattering patterns. The interpretation of the origin of this scattering is supported by the previously reported observation of the specimens during their deformation, indicating a strong whitening of the material at this level of strain, which suggests the formation of elongated microvoids in the sheared polymer. The shape and orientation of the SAXS patterns indicate that the microvoids are elongated in shape and that the orientation of their long axis is a few degrees away from the shear direction x_2, which is essentially the same as the orientation of the crystallographic c axis, as is evident from the pole figures for the 002 planes.

In the range of imposed shear strain studied here, the small-angle scattering by the lamellar structure quickly fades and finally, at $\gamma = 4.3$, it can no longer be distinguished in the scattering pattern. This may suggest the destruction or substantial reorganization of the lamellar structure.

Some additional information on the texture development in sheared HDPE is provided by the scattering experiments performed during sample deformation and subsequent strain recovery on unloading. The SAXS and WAXS patterns, taken viewing the samples along the x_3 axis (i.e. perpendicular to the shear direction), were recorded for the small specimens as they were deformed directly in the X-ray camera, as described earlier. The results for three samples are presented in *Figures 7–9*. For each sample the first set of SAXS and WAXS patterns (in the top of the figure) was obtained for the sample while still under load after the desired strain was attained ($\gamma = 0.67$, 1.0 and 2.0 for the samples represented in *Figures 7*, *8* and *9*, respectively). The second set of patterns was taken during the strain recovery process, 1 min after load release, while the last set was recorded 24 h after unloading when the strain recovery was nearly complete (the final strains reached after 24 h were then $\gamma = 0.16$, 0.52 and 1.40, respectively, for *Figures 7*, *8* and *9*). The first set of patterns in *Figure 7* represents the initial undeformed state.

The WAXS patterns shown in *Figures 7–9* suggest that the crystal texture under load is bimodal, comparable to that observed previously in relaxed samples at similar levels of strain (compare with the patterns presented in *Figure 5*). However, the diffraction peaks seem to be wider in samples under load than after load release, which indicates some straining and distortion of the crystal lattice in the loaded state and its subsequent relaxation

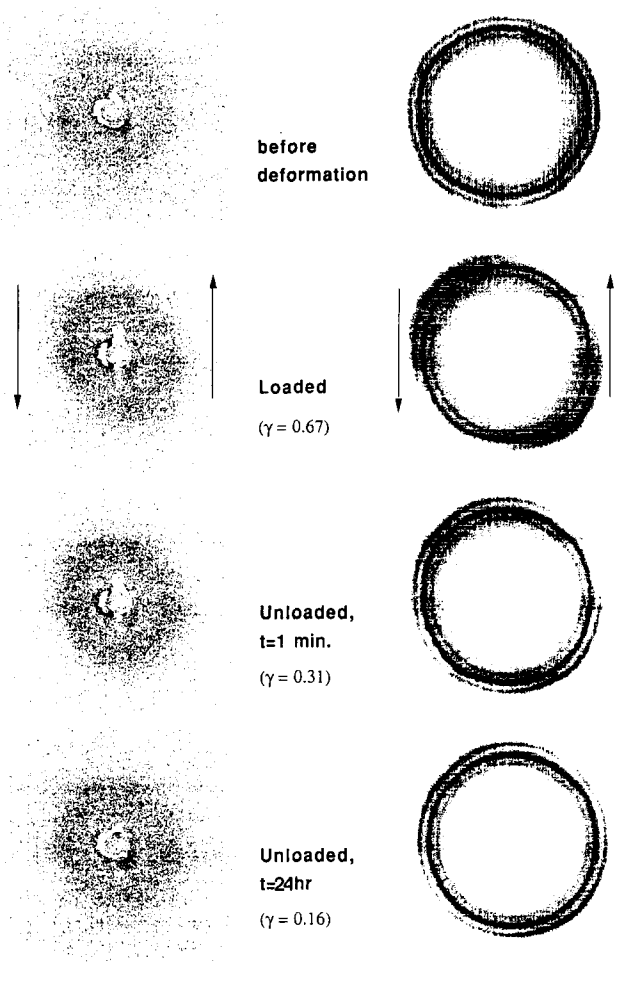

Figure 7 The SAXS (left) and WAXS (right) patterns as viewed from the x_3 direction of the shear specimen before deformation and deformed to a strain of 0.67. The patterns were recorded under load, 1 min after unloading and 24 h after unloading

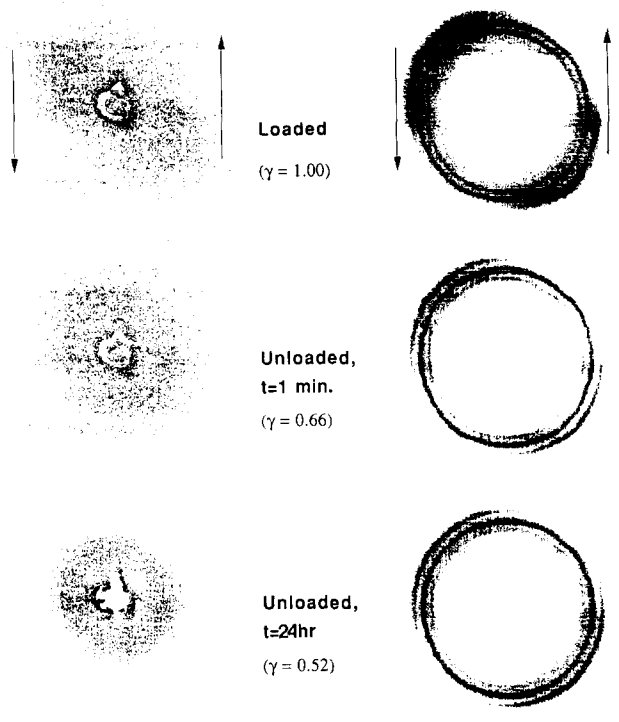

Figure 8 The SAXS (left) and WAXS (right) patterns as viewed from the x_3 direction of the shear specimen deformed to a strain of 1.0. The patterns were recorded under load, 1 min after unloading and 24 h after unloading

on unloading. After load release, one pair of arcs of the (110) and (200) reflections maintains its position near the equator of the WAXS pattern, while another rotates back about 10° towards the shear direction. Moreover, the length of both the (110) and (200) arcs increases on unloading, which indicates some decrease in crystal order during strain recovery. Such randomization of the crystal orientations on unloading is more noticeable in samples sheared to smaller strains (see *Figure 7*).

Figure 7 demonstrates that for a smaller shear strain (strain under load, $\gamma = 0.67$) the SAXS pattern changes from circular to elliptical, with the long axis oriented at an acute angle to the shear direction. The long axis of the ellipse is longer than the diameter of the ring observed for the undeformed sample, indicating a decrease in the longer period in that direction in the deformed state. No distinct maxima or minima of the intensity can be distinguished along the elliptical contour. The strain recovery induces reorientation and a change in the shape of the ellipse: it rotates backwards, with the long axis moving about 10° towards the shear direction, as does one set of reflections in the WAXS patterns. Simultaneously, the ratio of the lengths of the axes decreases, falling close to 1 at the end of the strain recovery process, which also demonstrates some randomization of the lamellar orientation distribution.

The lamellar structure changes further when the applied strain increases. In the sample sheared to an applied shear strain of 1.0 (*Figure 8*), the SAXS pattern recorded under load is of a two-point type, indicating clearly the development of a preferred lamellar orientation through deformation. This two-point pattern, however, transforms on unloading into an ellipse with an aspect ratio that decreases with time, which again suggests a substantial randomization of the lamellar structure during strain recovery. The orientation of the lamellae achieved in the deformation process is more stable on unloading if the sample was sheared to a higher strain of 2.0 (see *Figure 9*). In that case, the two-point character of the SAXS pattern persists also in the fully recovered sample. There is only a reverse rotation of the direction of preferred orientation (again about 10°) and some increase of the long period towards its initial value upon unloading of the sample, similar to the behaviour of the less-sheared samples.

The small samples deformed to high shear strains ($\gamma > 3.5$; scattering patterns not shown here) did not exhibit any scattering typical for a lamellar structure. This is in accordance with the results reported above for large samples, in which the scattering by the lamellar structure disappeared at a similar level of strain.

The SAXS patterns obtained from the small samples and presented in *Figures 7–9* do not show the strong equatorial scattering characteristic for the large samples (*Figure 6*). We should recall the observation reported in the previous section that the small samples did not whiten during shear and remained transparent up to a high shear strain, which is opposite to the behaviour of the large samples. Both observations indicate that cavitation was absent or very limited in the case of the small samples. As we discussed before, the reason for such a difference in sample behaviour lies, most probably, in the difference between the length to width ratios of the narrow shear zones for both sample types; a high ratio limits the end effects on the deformational behaviour in the central part of the specimen, and apparently suppresses cavitation.

Morphology changes

Figures 10a–f show TEM micrographs of ultrathin sections of undeformed (*Figure 10a*) and sheared (*Figures 10b–f*) HDPE stained with chlorosulfonic acid[9].

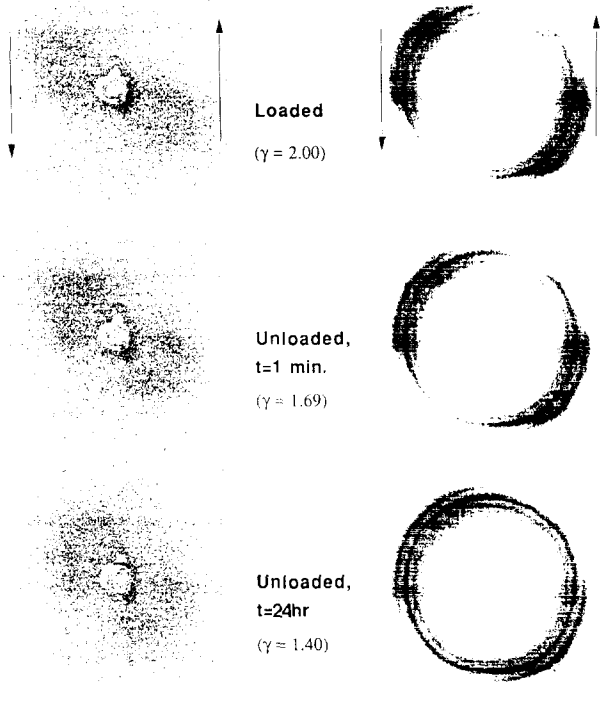

Figure 9 The SAXS (left) and WAXS (right) patterns as viewed from the x_3 direction of the shear specimen deformed to a strain of 2.0. The patterns were recorded under load, 1 min after unloading and 24 h after unloading

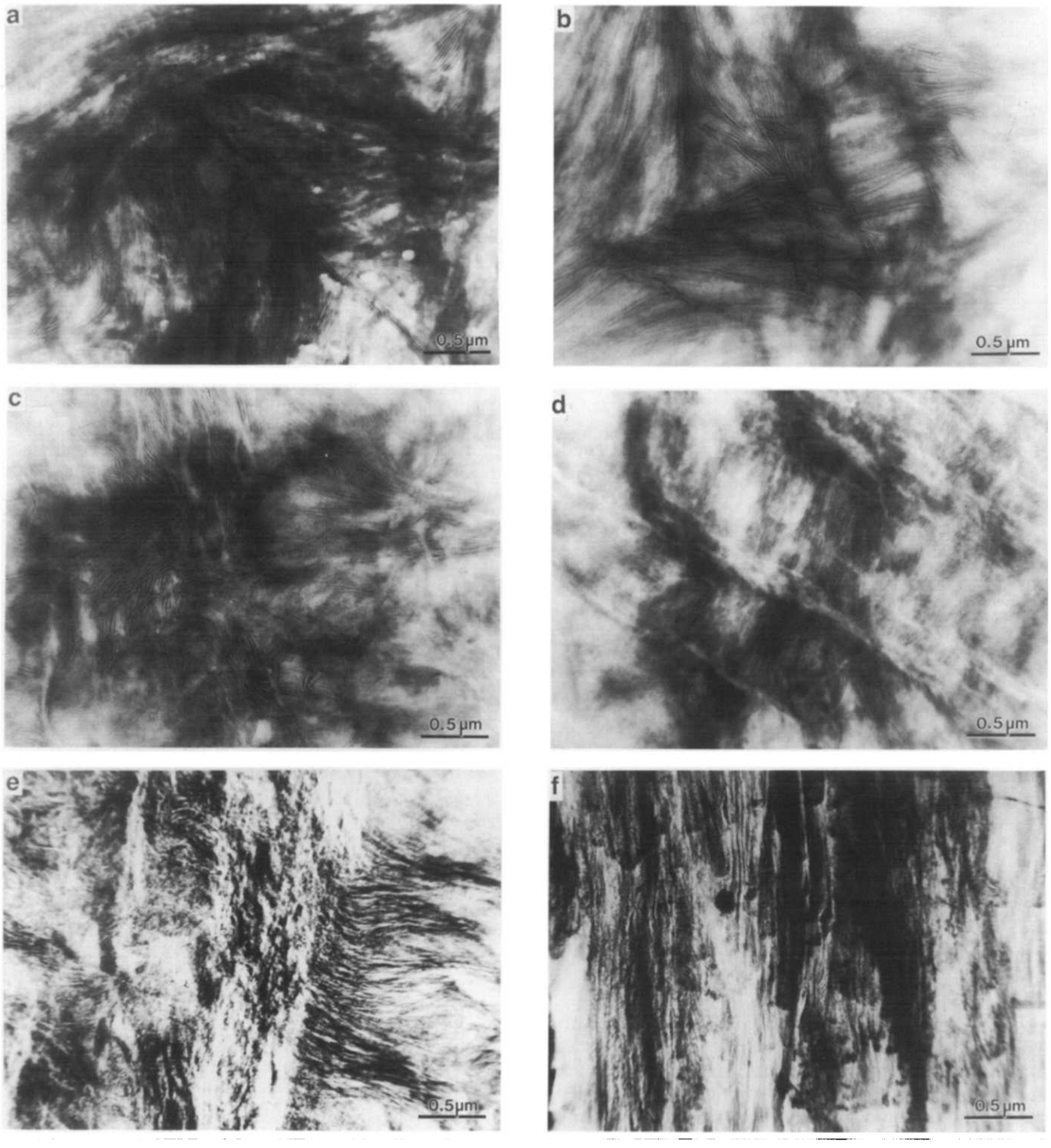

Figure 10 Transmission electron micrographs of ultrathin sections cut along the x_1–x_2 plane from (a) undeformed HDPE and HDPE sheared to a permanent strain of (b) 0.42, (c) 1.0, (d) 1.8, (e) 3.0 and (f) 4.3

The sections were cut perpendicular to the x_3 axis from the large samples used previously in the X-ray structural studies.

Figure 10a shows that in the undeformed HDPE the orientation of the lamellae is random. At a relatively low shear strain ($\gamma = 0.42$; *Figure 10b*), again no particular preferred lamellar orientation can be detected, and the lamellar structure resembles approximately that for the undeformed sample. A new characteristic of the morphology can be detected in the section of the sample deformed to a permanent shear strain of 1.0. At this strain a few very fine deformation bands can be seen in the micrograph. These bands are approximately parallel to the shear direction and usually run across the stacks of lamellae which are oriented more or less perpendicular to the direction of shear. The bands are few and are well separated one from another. The orientation of the bands in relation to the lamellae suggests that they were formed by localized shear in the lamellae along the direction of the molecular axis c. The length and number of these bands increases markedly with increasing strain. In the micrograph of the sample deformed to $\gamma = 1.8$ (*Figure 10d*), one can find a collection of long, relatively densely packed deformation bands, all

oriented approximately along the shear direction. These fine deformation bands are, however, still separated. *Figure 10e* ($\gamma = 3.0$) shows further development of the sample morphology with increasing strain. The density of the deformation bands has now increased to such a level that they tend to coalesce and form much thicker bands. The lamellar morphology inside these bands appears to be completely destroyed and replaced by a fibrillar morphology. At a shear strain $\gamma = 4.3$, the deformation bands have multiplied and spread over the whole sample (see *Figure 10f*). The transformation of the morphology from lamellar to fibrillar is practically complete at this deformation stage, and only in very few places of the micrograph do some traces of the old lamellar morphology remain. These remnants are in the form of clusters of three to four very short fragments of adjoining lamellae. The micrograph in *Figure 10f* shows that the short lamellae forming a cluster are terminated on both ends by nearby fine shear deformation bands, which suggests that they originate from the initially long lamellae, fragmented and mostly destroyed by the developing shear deformation bands. These lamellar fragments are tilted towards the direction of the bands more than were their predecessors at lower strains. This indicates the presence of intense shear along the chain direction inside these lamellar remnants. Finally, this shear leads to a complete disintegration of any traces of the initial lamellar morphology at strains higher than 4.3.

The destruction of the lamellae and the transformation of the sample morphology were not unique for large samples deformed in the Instron, in which the end effects were substantial. The same type of transformation was also observed by means of TEM in the small samples, in which the influence of the end effects on the shear deformation in the central part of the specimen was quite limited. This demonstrates that the abrupt transformation of morphology is an intrinsic feature of the deformation of HDPE by shear and is not related to cavitation induced by end effects.

DISCUSSION

The experimental results presented in the previous section show that the method of deformation of HDPE used in the present study does not produce a pure mode of macroscopic simple shear deformation in the entire narrow shear zone of the large specimens with a relatively small aspect ratio in this narrow zone. Tensile and compressive deformations also develop at the ends. However, in the central part of the specimen, far from its ends, the deformation process can be considered as a reasonable approximation to a simple shear deformation mode. In the smaller specimens with larger narrow gauge aspect ratios, the deformation was far closer to a simple shear mode. All the structural studies reported here were carried out using only these central parts of the deformed specimens; thus, in our opinion, the results obtained refer exclusively to the plastic deformational behaviour of HDPE in simple shear. Nevertheless, the results for the large scale specimens are not entirely free of spurious effects, as we have already pointed out above.

Using the coordinates defined in *Figure 1*, the finite deformation of a solid in planar simple shear can be described by a set of linear affine transformation equations

$$x_1 = X_1$$
$$x_2 = X_2 + \gamma(t) X_1$$
$$x_3 = X_3 \qquad (1)$$

where X_i and x_i are the coordinates of the material points before and after deformation, respectively, and $\gamma(t)$ is the shear strain at time t. The linearity of the equations reflects the homogeneity of the deformation. During the simple shear deformation the principal axes of the strain ellipsoid (principal directions of the finite strain tensor) rotate monotonically with increasing shear strain γ towards the shear axis x_2. The angle α between the major principal axis of extension and the shear axis is given by[11]

$$\alpha = \tfrac{1}{2}\cot^{-1}(\gamma/2) \qquad (2)$$

The value of α decreases with γ, starting from $\alpha = 45°$.

Equations (1) and (2) are valid for isotropic materials. The unoriented HDPE with a spherulitic morphology, used in this study, may be considered as isotropic only on the macroscopic average level. On a microscopic scale, however, it consists of highly anisotropic elements, each formed by lamellar crystals coupled with adjoining amorphous layers oriented randomly in the material. Experimental results show that the deformation of HDPE in simple shear is macroscopically homogeneous and obeys equations (1) and (2) on the average. Nevertheless, the deformation results from the superposition of a series of local non-homogeneous deformations of the anisotropic elements. Activation of the appropriate deformation mechanisms and the resulting deformation path of any particular structural element is controlled by its orientation with respect to the applied stress axis and the orientation of the surrounding elements in relation to the stress axis.

The results of the structural studies suggest that in the initial stages of the plastic deformation of spherulitic HDPE ($\gamma = 0.08$ and 0.16), the deformation of lamellar crystals proceeds mainly by shear along the 100 crystallographic planes of these crystals. The crystallographic deformation mechanisms available for such shear are the (100)[001] chain slip (crystallographic slip on the 100 plane along the chain direction [001]) and (100)[010] transverse slip (slip in the same plane but in the [010] direction, perpendicular to the chain direction). These two mechanisms are known as the easiest ones to activate slip deformation in the orthorhombic polyethylene crystals. The critical resolved shear stresses for these systems are 7.2 MPa and 12.2 MPa, respectively[12]. Slip activity in these mechanisms involves lattice rotation of the deformed crystals[10,13], which in turn leads to development of the deformation textures observed in *Figures 5a* and *5b*. The orientation distribution of the crystallographic a axis (normal to the 100 planes) forms an apparent maximum in the direction close to the minor axis of the macroscopic strain ellipsoid (direction of maximum compression), whereas the distributions for the b and c axes start to form low and broad maxima somewhere near the direction of the major axis of this ellipsoid (direction of maximum stretch) as the deformation develops. The size of the orientation maxima suggests that in the initial stages of macroscopic deformation the activity of these mechanisms is probably limited to those crystals which are already properly oriented for a particular slip, i.e. the

resolved shear stresses on their 100 planes are sufficiently high to activate slip. The decrease in the thickness of sheared lamellae is a product of the (100)[001] chain slip, and can be observed experimentally by SAXS as the decrease in the long period measured along the direction of the short axis of the macroscopic strain ellipsoid (see *Figure 6*).

The deformation by crystallographic slip operations on the 100 plane of the crystals must be accompanied by simultaneous shear of the amorphous interlamellar layers (interlamellar sliding) by reasons of compatibility. This deformation mode operates in the amorphous phase, which in HDPE at room temperature is of a rubbery nature with a resistance lower than that of any crystallographic slip. Its activity helps to produce the preferred orientation of the lamallae normals along the minor axis of the macroscopic strain ellipsoid. The SAXS patterns for samples deformed to small strains, recorded under load as well as after load release (see *Figures 6* and *7*), do not exhibit very distinct maxima, which suggests that the interlamellar sliding is not intense enough or well enough organized at this early deformation stage. On the other hand, the SAXS and WAXS patterns recorded after load release indicate that the crystallographic and lamellar textures change in a similar manner on unloading: both patterns rotate together in the same direction and show some randomization of the texture (see *Figure 7*). These changes are accompanied by some recovery of overall macroscopic strain (see *Figure 4*). Such behaviour could not result from the reversal of crystallographic slip on unloading; the principal cause is rather the relaxation and strain recovery in the strained amorphous layers by the reversal of interlamellar sliding[4,13,14], which in view of the rubbery nature of this material should not be difficult. This clearly indicates that during the deformation process the interlamellar shear had to be active as one of the deformation mechanisms. The same interlamellar shear was also found to be partially reversible on unloading in uniaxially compressed HDPE[5]. Because of the low overall shear strain the interlamellar shear on loading is not very intense at this early deformation stage. Molecules in the amorphous layers extend, but stretch only to a limited extent as they lock eventually during interlamellar shear. Consequently, the amorphous material is potentially able to recover the strain almost entirely upon unloading. This is illustrated in *Figure 4*, which shows that for an applied strain up to 0.7 most of the inelastic strain is recovered upon sample unloading. However, while the interlamellar shear intensifies markedly, its ability to recover on unloading is strictly limited at higher shear strains owing to its locking behaviour mentioned above. This aspect will be discussed further below.

At a permanent shear strain near $\gamma = 0.42$, the maxima of orientation distributions of both *b* and *c* axes become better defined than at lower strains and apparently change their positions. A maximum of the *b* axis orientation moves towards the centre (x_3), while the *c* axes of the crystals move to the equatorial plane of the pole figure (x_1–x_2 plane) and tend towards the x_2 axis of shear, as shown in *Figure 5c*. These changes follow from a joint rotation of both *b* and *c* crystallographic axes around the direction of maximum orientation of the *a* axis. Such rotation suggests an activation of the (010)[001] chain slip in addition to the already active (100)[001] and (100)[010] slip processes. The critical resolved shear stress for the (010)[001] chain slip[12] is 15.6 MPa, which is significantly higher than the plastic resistances of the two slip systems on the (100) plane, and therefore the activation of this third slip system requires higher shear stresses than the slips acting in the 100 plane.

Examination of the WAXS and SAXS patterns of *Figures 5* and *6* shows two related and important textural alterations with increasing shear strain. First, we note that at permanent shear strains above 0.42 a clear bimodal crystallographic texture starts to emerge which lasts until a shear strain in excess of 3.00 is reached (see *Figures 5c–f*; $\gamma = 0.42$–1.8). Of these, the primary texture element is oriented with its *c* axis tilted a little away from the macroscopic shear direction x_2 towards the direction of maximum stretch in the x_1–x_2 plane, with the *a* axis being in the same plane and the *b* axis oriented around the x_3 axis. This orientation mode is dominant and stable: it does not rotate relative to the x_2 axis with increasing strain. Upon unloading of the sample the centre of the *c* axis cluster rotates away from the x_2 axis by a small angle. In contrast, the second texture element, oriented with its *c* axis cluster at larger angles away from the x_2 shear axis in the direction of maximum tension, rotates gradually towards the x_2 axis with increasing shear strain. Upon unloading, the centre of this secondary *c* axis cluster also rotates back away from the x_2 direction, i.e. the (110) and (200) poles rotate towards the direction of shear, as can be seen in the WAXS patterns shown in *Figures 8* and *9*. This reverse rotation is stronger than the corresponding rotation of the primary *c* axis cluster.

The reasons for the formation of such a bimodal orientation of the crystallites are not entirely clear. Nevertheless, a possible scenario can be constructed. First, the stronger, primary orientation mode originates most probably from the activity of the previously discussed crystallographic deformation mechanisms, mostly by (100)[001] chain slip. The deformation of the initially most favourably oriented crystallites by the easiest (100)[001] chain slip, accompanied by less intense (100)[010] transverse slip and (010)[001] chain slip, results in a rotation of the (100) planes towards an orientation perpendicular to the x_1–x_2 plane (normals rotating in the x_1–x_2 plane towards the x_1 direction) with the *c* axes aligning in the direction of maximum stretch (maximum tensile stress). At the same time, the lamellar normals rotate in the opposite direction, i.e. towards the direction of minimum stretch (maximum compressive stress), as should be expected for deformation by chain slip[13]. The intensity of the (100)[001] slip activity depends on the resolved shear stress on the 100 plane in the [001] direction, which in turn depends on the orientation of the crystal in the macroscopic shear field. This driving stress reaches its maximum value when both the plane normal and the slip direction vector make a 45° angle with the direction of principal applied stress and decreases when either of these two angles departs from 45°.

As the shear deformation develops, in the early phase, for shear strains up to $\gamma = 3.0$ in all crystallites which are favourably oriented to have a high resolved shear stress, the principal slip activity on the 100 planes tends systematically and monotonically to rotate the 100 plane normals towards the x_1 axis and the *c* axis directions towards the shear direction x_2. Once the planes have reached this state their *c* axes add to the principal textural

cluster which remains stably locked in its position, since for those crystallites lattice rotations relative to the x_2 axis cease. In this process the b axis orientations of all such crystallites tend to migrate towards the x_3 direction. Within this stage of deformation the primary textural cluster behaves as the main trend in plane strain compression[4]. Thus, in all of this texturing process the orientation distribution of the c axes in the primary cluster becomes tighter as the deformation develops and the scattered intensity increases.

The formation of a second orientation mode observed in the pole figures results, in our opinion, from the shear deformation of the interlamellar amorphous layers (interlamellar sliding). The activity of this deformation mode induces rotation (reorientation) of the entire lamellae but does not influence the angle between the lamellar normal n and the c axes. Through this interlamellar shear the lamellar normals rotate towards the direction of minimum stretch. As already discussed, at small shear strains (permanent strain $\gamma < 0.42$) the interlamellar sliding was only partially developed and was almost completely reversible upon unloading. Later, most of the incremental plastic deformation takes place by crystallographic slip, and then mostly in those crystals already favourably oriented to be subjected to high resolved shear stress for a particular slip system rather than other mechanisms. This deformation process that opposes the main texture development prevents some crystallites from shearing and undergoing the same strains as the main group. Later, with increasing overall strain, when the finite interlamellar shearing capacity is exhausted by locking of the stretched tie links, the previously misoriented lamellae also become available for chain slip and other crystallographic slip modes. Then the secondary texture gradually dissolves and is added to the primary texture. The adverse rotation of undeformed lamellae by interlamellar shear peaks around an applied shear strain of about 1.0 (which corresponds to a permanent strain near 0.5; see *Figure 8*). The saturation of the recoverable shear shown in *Figure 4* is a direct result of the locking of the amorphous material. Upon unloading the total strain recovery comes primarily from the reversal of this interlamellar shear. Thus, above the applied strain of 0.7 the amount of recoverable strain stabilizes at a constant level independent of the applied strain. Beyond this point the primary texture continues to develop by a tighter clustering of all c axis orientations and their increasingly closer approach towards the x_2 axis. In this region of intermediate strain around 3.0 the a and b axes tend towards the x_1 and x_3 axes, respectively, and the simple shear texture resembles crudely the much better defined plane strain compression texture explored by us earlier[4]. In this range of intermediate strain, where the amorphous material has fully sheared and locked, the amorphous layers rotate while attached to the lamellae and the layer normals n group together weakly and rotate towards the x_1 axis (remaining nearly normal to the c axes and nearly parallel to the a axes in the intensely sheared lamellae). This long period reorientation can be readily perceived in the small samples in *Figure 9* (at $\gamma = 2.0$). In the large samples, which undergo extensive whitening, this lamellar rotation is masked by the much more intense scattering coming from the cavities.

The morphological observations by TEM, supported by SAXS results, demonstrate that in the intermediate range of shear strain (permanent strain $\gamma \geqslant 1.8$) the deformation of the polymer becomes unstable on a fine scale and localizes in fine shear bands running along the chain directions across several adjoining lamellae. The orientation of these bands suggests that they result from localized intense chain slip in lamellar crystals. These shear bands, initially widely dispersed, quickly multiply and merge together when the strain increases, forming much wider bands. At a permanent strain near 3.0, the shear inside these bands dominates in the deformation of the polymer, as can be seen in *Figure 10e*. The intense chain slip within the bands, most probably made up of the easiest (100)[001] chain slip, induces extensive fragmentation of the lamellar crystals and results in a consequent transformation of the lamellar morphology into a microfibrillar morphology. As a result of the fragmentation of lamellae, the small blocks of very short lamellar remnants become unconstrained and rotate readily about their c axes, allowing the easier crystallographic slip systems to become freely active. This new freedom is the principal cause for the eventual development of the fibrous texture. The multiplication and development of the shear bands, as well as the intense slip within the reoriented lamellar remnants, lead to a nearly complete unravelling of the initial lamellar morphology at a permanent strain near 4.3 (*Figure 10f*). Neither TEM nor SAXS reveals any recognizable traces of a lamellar structure above this strain. Whatever lamellar structure that might have remained is not now detectable by TEM and is masked in SAXS by the more intense scattering from the voids that produce whitening. The intense slip in deformation bands and the resulting transformation of the sample morphology now induce the change in the crystallographic texture of the deformed polymer. The secondary texture element produced at earlier deformation stages by interlamellar sliding declines in concentration and finally disappears near a permanent strain $\gamma = 4.3$. Because of the transformation to a microfibrillar morphology, as discussed in connection with the TEM observations, the crystals continuously deforming by slip are markedly reduced in size and are much less constrained. At this stage any small tendency towards rotation of the fibrils being sheared past each other finds little resistance and can result in favourable orientation of the remaining, previously not fully deformed crystallites by random rotation of fibrils about their c axes. This causes the development of the eventually dominant fibrous texture with axial symmetry along the chain direction of the crystals. The orientation distribution of the chain axis c now becomes very sharp owing to the increased, unconstrained activity of chain slip. The orientation maxima of the poles of the ($hk0$) planes elongate within the plane perpendicular to the maximum of c because of possible rotations of the less-constrained crystals. At $\gamma = 6.3$ the distribution of these poles in the plane perpendicular to c is much flatter and random than at lower strains, although the outlines of the old orientation maxima can still be recognized (see *Figure 5i*).

As we mentioned before, the formation of the shear bands and destruction of the lamellar morphology in the case of the large specimens were accompanied by intense cavitation of the polymer. This phenomenon, in our opinion, is not a fundamental ingredient of the deformation of HDPE by simple shear, but rather results from the sample geometry that permits end effects of

relatively far-reaching influence, resulting in spurious deformation modes at the ends of the narrow shear zones. In the case of the small specimens, where the end effects were very localized because of proper sample geometry, the transformation between lamellae and microfibrils was not accompanied by the cavitation process and the polymer morphology resulting from undisturbed shear deformation was relatively free of microvoids.

The transformation of the sample morphology during simple shear deformation somewhat resembles the transformation observed during neck formation in the tensile deformation of HDPE, including the development of the fibrous texture and even some spurious cavitation. On the other hand, during plastic deformation of HDPE by compression[4,5] or rolling[10,15], the lamellar morphology is preserved up to very large strains in spite of slip instabilities and localization of the deformation into deformation bands occurring under plane strain compression at a similar level of strain[4]. In these deformation modes, where a superposed pressure is present, such spurious phenomena resulting from local tensile stresses are suppressed, whereas in the case of deformation by shear no such superposed pressures are present and tensile stresses generated by end effects have far-reaching consequences. One such consequence is the relatively more ready transformation of the morphology from lamellar into microfibrillar. In a separate communication[16], we have used a new computer simulation of the texture evolution, developed by Lee *et al.*[17], to assess our experimental findings reported here. This simulation has provided valuable insight into the complex processes discussed here.

We note that in simple shear, where an eventual stable fibrillar texture evolves with a propensity for almost limitless shear deformation at a steady state, the destroyed lamellar morphology is not replaced by a new, restructured long period as was the case in the irrotational flow fields of uniaxial tension, plane strain compression and rolling. Why this is so is not entirely clear. In the case of plane strain compression, where Galeski *et al.*[4] made a detailed observation of the series of processes that lead to the restructuring of a new long period, it has been proposed that there is a widespread pinch-off of the stretching lamellae when the interface stretching resistance becomes comparable to the plastic resistance of the lamellae. Then, apparently, the fragments of crystallites can form a new long period by interface migration (migration of chain defects along chains), which redistributes the previously associated defects in chain packing, making up amorphous material into a new arrangement that remains stable on the stretched out molecules aligned in the irrotational principal direction of extension and thereby reduces the interface energy. In simple shear this does not occur for two possible reasons. First, any tendency to minimize the interface area between crystallite and amorphous regions by rotation of the interface (migration of chain defects along chains) would be counteracted by the shear parallel to the aligned molecules. Second, the fragmentation of lamellae into fibrils on a fine scale may accomplish the rejection of defects in chain packing into the interfibrillar zones, eliminating any need to segregate them into planar zones. A more definitive treatment of this subject would require a degree of understanding and a means of treatment of the forms of topological transformations of macromolecules undergoing relative motion in a solid which presently do not exist.

Finally, a comparison might be made of our present and earlier work with the rolling study of Krause and Hosford[18], even though their maximum equivalent strain level of 1.36 is far smaller than our maximum equivalent strain level of 6.3 for which the fibrous texture develops, and the two processes of deformation are radically different kinematically. A more appropriate comparison of the Krause and Hosford research is with our plane strain compression experiment, which was carried out for equivalent strains up to 2.5. In neither the plane strain compression experiment nor the simple shear experiment, however, was much evidence found for the activity of (110)[001] chain slip which Krause and Hosford report for simple shear. The prominent systems were (100)[001] and (010)[001], with only a trace of (110)[001] observable. This observation is reinforced by the experiments in which slip resistances of individual systems were measured in blocks cut out of quasi-single-crystal textured samples. In these, (110)[001] slip could not be developed because of the lower resistances on other available and better slip systems, in spite of their much lower Schmid factors. It is quite possible that in the rolling experiments, where considerable friction-induced redundant deformation is possible, the (110)[001] system could indeed be active as reported by Krause and Hosford.

CONCLUSIONS

On the basis of the experimental results presented in this work, the following conclusions can be drawn.

1. The plastic deformation of HDPE by planar simple shear carried out at room temperature is locally not a pure process but is composed of a complex sequence of deformation phenomena occurring at various stages of the deformation and controlled by various deformation mechanisms developing in a special sequence.
2. At low and moderate shear strains (up to $\gamma = 3.0$), the plastic deformation is controlled by crystallographic deformation mechanisms. Among these mechanisms the (100)[001] chain slip is the most important, being active from the very beginning of the deformation process. Other, less active deformation mechanisms include the (100)[010] transverse slip and (010)[001] chain slip systems. No evidence for the activity of other slip systems, twinning or martensitic transformations was found.
3. Plastic deformation by crystallographic mechanisms is accompanied by shear of the amorphous material, resulting in interlamellar sliding. This deformation mode is most active at moderate strains and additionally appears to be extensively reversible upon unloading. This leads to the recovery of a fixed part of the non-elastic strain on unloading. Simultaneous activity of crystallographic mechanisms and shear in the amorphous layers leads to the formation of a bimodal orientation texture in the crystals, observed for permanent shear strains above 3.0.
4. In the range of moderate shear strains ($\gamma = 1.4$–1.8), the (100)[001] chain slip tends to localize because of slip instabilities and leads to the formation of fine

shear bands running across lamellae. With increasing strain these bands grow significantly in number. The shear within numerous deformation bands causes fragmentation of lamellae and their eventual destruction. As a result, the morphology of the material transforms from lamellar to microfibrillar at a permanent strain near 4.3. The slip instabilities leading to the generation of deformation bands appear in the material when the slip in the crystals is advanced. The resulting transformation of the lamellar crystals into microfibrils is similar to that observed in tensile deformation. This transformation can be accompanied by widespread cavitation of the deformed polymer, causing whitening of large samples with prominent end effects. This mode of cavitation, however, is not an essential feature of the deformation by shear but is rather a spurious side effect induced by the unwanted tensile deformations in the large samples with a small aspect ratio in the narrow shear zone. Such effects were absent in small samples with negligible end effects.

5. The transformation of the sample morphology and further intense slip in the crystals organized as microfibrils result in the formation of a final fibrous texture for the sheared HDPE as a single-mode texture with a sharp orientation of the crystallographic *c* axis, tilted away a little from the shear direction, and much wider orientation distributions of the *a* and *b* axes in the plane perpendicular to *c*.

ACKNOWLEDGEMENTS

This research was supported in part by a DARPA URI programme under ONR contract N00014-86-K-0768 through MIT and by the Centre of Molecular and Macromolecular Studies, Polish Academy of Sciences, Lódź, Poland.

REFERENCES

1 Bowden, P. B. and Young, R. J. *J. Mater. Sci.* 1974, **9**, 2034
2 Haudin, J. M. in 'Plastic Deformation of Amorphous and Semi-crystalline Materials' (Eds B. Escaig and C. G'Sell), Les Editions de Physique, Paris, 1982, p. 291
3 Lin, L. and Argon, A. S. *J. Mater. Sci.* 1994, **29**, 294
4 Galeski, A., Bartczak, Z., Argon, A. S. and Cohen, R. E. *Macromolecules* 1992, **25**, 5705
5 Bartczak, Z., Cohen, R. E. and Argon, A. S. *Macromolecules* 1992, **25**, 4692
6 Peterlin, A. *J. Mater. Sci.* 1971, **6**, 490
7 G'Sell, C., Boni, S. and Shrivastava, S. *J. Mater. Sci.* 1983, **18**, 903
8 Dahoun, A., G'Sell, C., Philippe, M. J. and Esling, C. in 'Proceedings of 8th International Conference on Deformation, Yield and Fracture of Polymers', Plastics and Rubber Institute, London, 1991, pp. 68, 1–4
9 Kanig, G. *Kolloid Z. Z. Polym.* 1973, **251**, 782
10 Song, H. H., Argon, A. S. and Cohen, R. E. *Macromolecules* 1990, **23**, 870
11 Jaeger, J. C. 'Elasticity, Fracture and Flow', Chapman & Hall, London, 1969
12 Bartczak, Z., Argon, A. S. and Cohen, R. E. *Macromolecules* 1992, **25**, 5036
13 Young, R. J., Bowden, P. B., Ritchie, J. M. and Rider, J. G. *J. Mater. Sci.* 1973, **8**, 23
14 Pope, D. P. and Keller, A. *J. Polym. Sci., Polym. Phys. Edn* 1975, **13**, 533
15 Frank, F. C., Keller, A. and O'Connor, A. *Philos. Mag.* 1958, **3**, 64
16 Lee, B. J., Argon, A. S., Parks, D. M., Ahzi, S. and Bartczak, Z. *Polymer* 1993, **34**, 3555
17 Lee, B. J., Parks, D. M. and Ahzi, S. *J. Mech. Phys. Solids* 1993, **41**, 1651
18 Krause, S. J. and Hosford, W. F. *J. Polym. Sci. B* 1989, **27**, 1867